Naples Shipping Week

TEMPESTE ESTREME

Aspetti tecnici, gestionali ed assicurativi

27 Settembre 2022 ore 14.00
Stazione Marittima di Salerno

SICUREZZA DELLE STRUTTURE PORTUALI: INFLUENZA DELLE ONDE ESTREME

Guido Benassai
Dip. Di Ingegneria, Università di Napoli Parthenope

INTRODUCTION - 1

Breakwaters play a crucial role in the protection of coastal zones. They are usually classified in **rubble mound breakwaters** and **vertical wall breakwaters**.

Depending on the local availability of materials, on the bathymetric conditions, on the wave climate and on specific design requirements, **rubble mound breakwaters** can be built by using rocks or concrete units, located as a double or single layer, considering a traditional trapezoidal shape or a berm breakwater, with different types of toe structures.

Concerning rubble mound structures, **damage of an element** can be defined as the partial or total loss of its functionality. The concept of damage is usually related to the hydraulic instability of the armor layer. It is commonly utilized to refer to the geometrical evolution in comparison with the "undamaged" section and, occasionally, also to the breakage of armor units. With reference to the damage measurement, in hydraulic laboratories itis generally performed through mechanical or laser profiling [9–13] or visually by means of video cameras.

In the following, a novel technique proposed by Musumeci et al (2018) based on RGB-D cameras will be described to measure rubble-mound breakwater damage. The method was applied to the investigation of the stability of an Accropode breakwater under wave attack. The breakwater section was reinforced with a berm to increase the structure safety against extreme waves.

INTRODUCTION - 2

Vertical wall breakwaters are generally built on higher depths, in the past they were constructed with cyclopic concrete units, from 1950's they are built with monolithic caissons.
Damage of an element consists essentially in the sliding of the caisson. In fact a vertical caisson breakwater has several modes of failure, but **the primary cause of damage is sliding** of the caisson (Goda and Takagi 2000; Takahashi et al. 2000). Therefore, caisson sliding is considered as the principal failure mode.
Burcharth (1998) analyzed safety aspects primarily related to **monolithic caisson structures** and presented a partial safety factor system for overall stability failure modes (Burcharth 2002).
During the past decade, the **performance-based design method** was developed, which allows a certain amount of sliding during the lifetime of a breakwater (Shimosako and Takahashi 2000; Goda and Takagi 2000; Goda 2001; Kim and Takayama 2003; Hong et al. 2004).
In the following, inclusion of the effects of the extreme waves and the climate change on the performance-based design of a caisson breakwater will be shown.
The effect of the climate change is taken into account for both extreme waves and storm surge. Max significant wave height at the storm peak are increased by 10% to take into account the wind speed increase of the monsoon winds, while the storm surge (which is added to the tidal excursion) is accounted for increasing the SWL by 10% of the SWH. By increasing the caisson width, the method gives also a procedure to increase the structure safety against extreme waves.

INDICE

http://meteo.uniparthenope.it

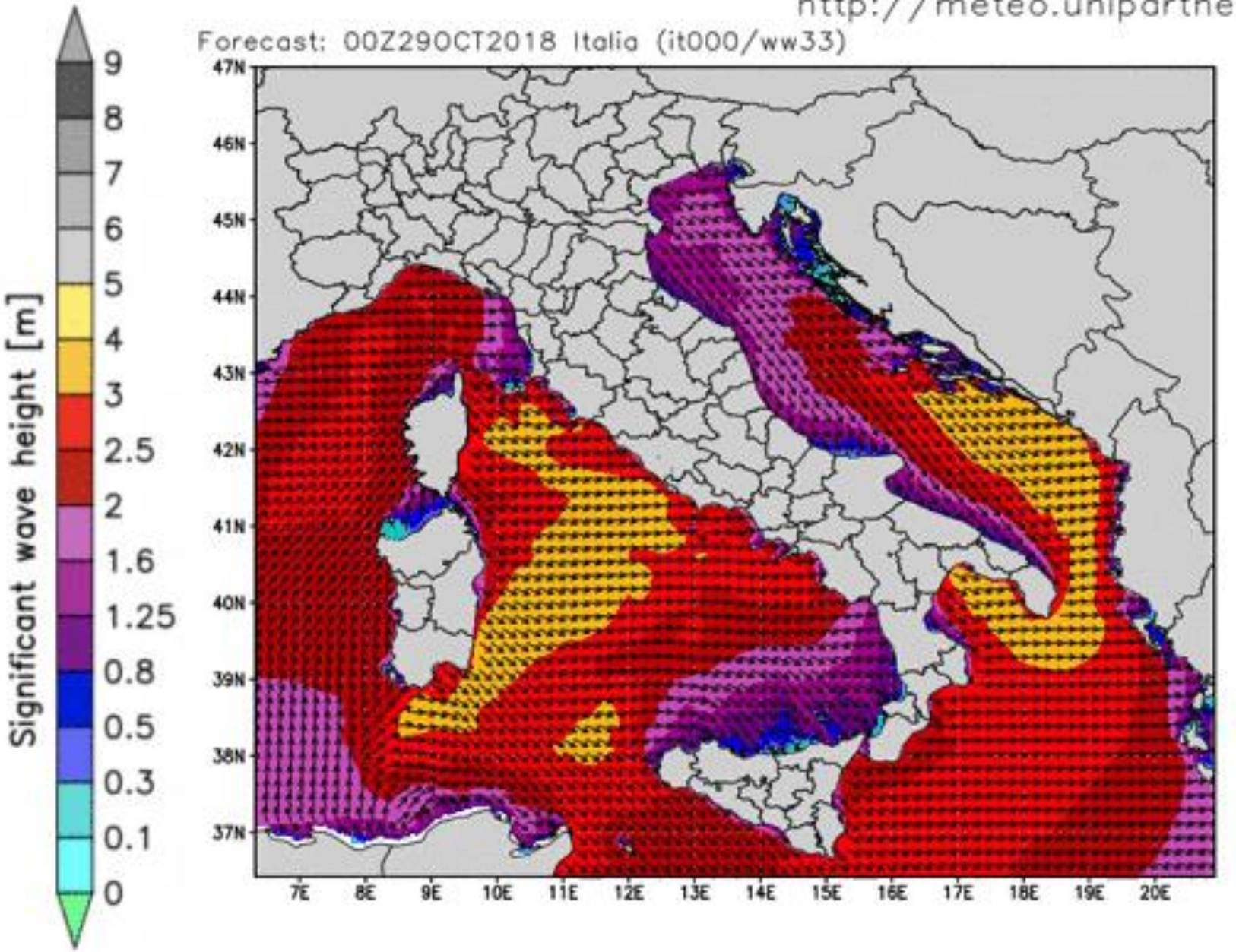

Danni riportati dall'evento 29-31 ottobre 2018: Pre-post evento Porto di Rapallo

Inabissamento natanti Porto di Rapallo

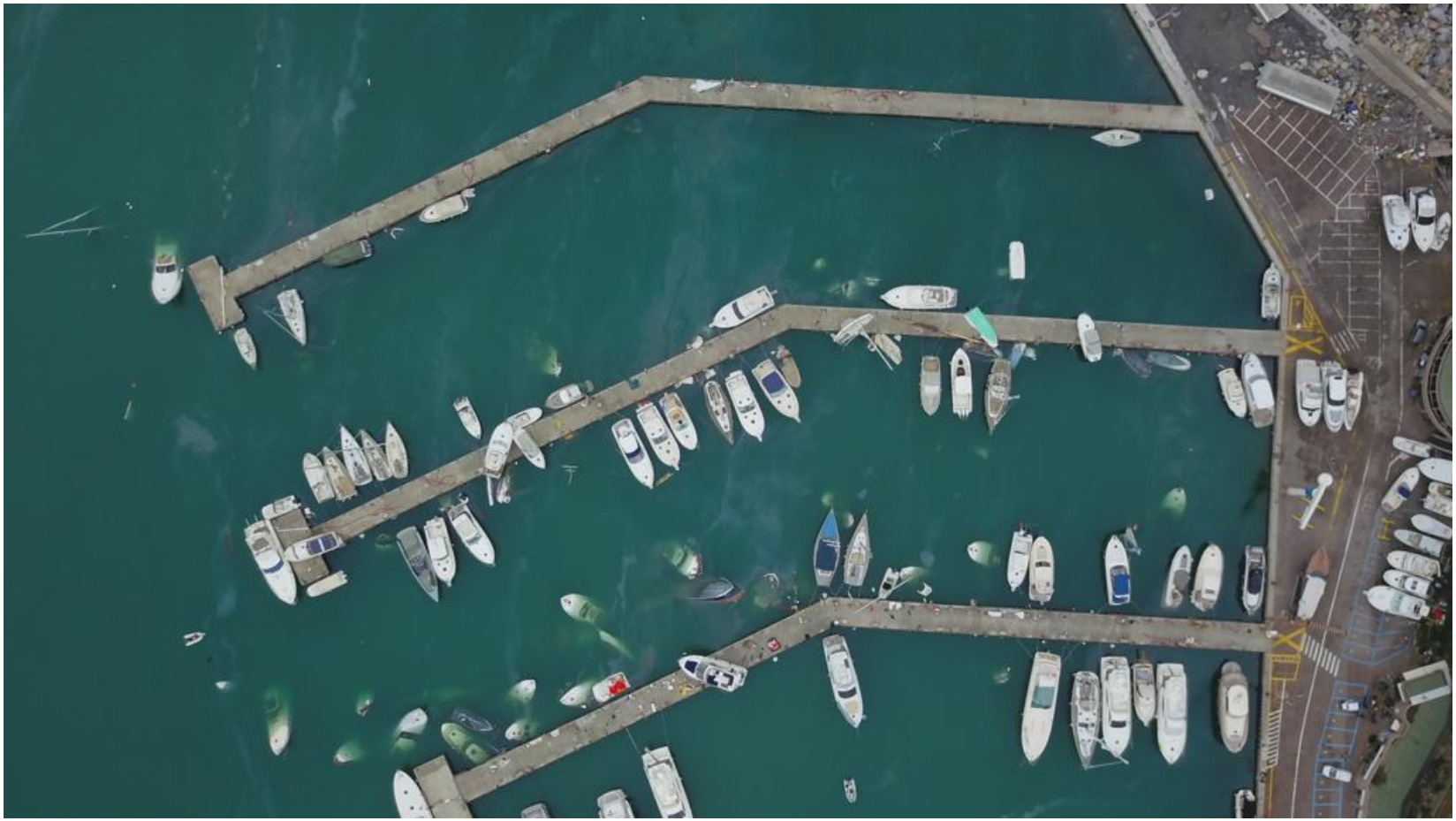

Prima dell'impatto dell'onda

Danni prodotti dalla mareggiata VAIA sulla diga foranea del porto di Rapallo

Danni prodotti dalla mareggiata VAIA
sulla diga foranea del porto di Rapallo

Frattura muro paraonde diga foranea

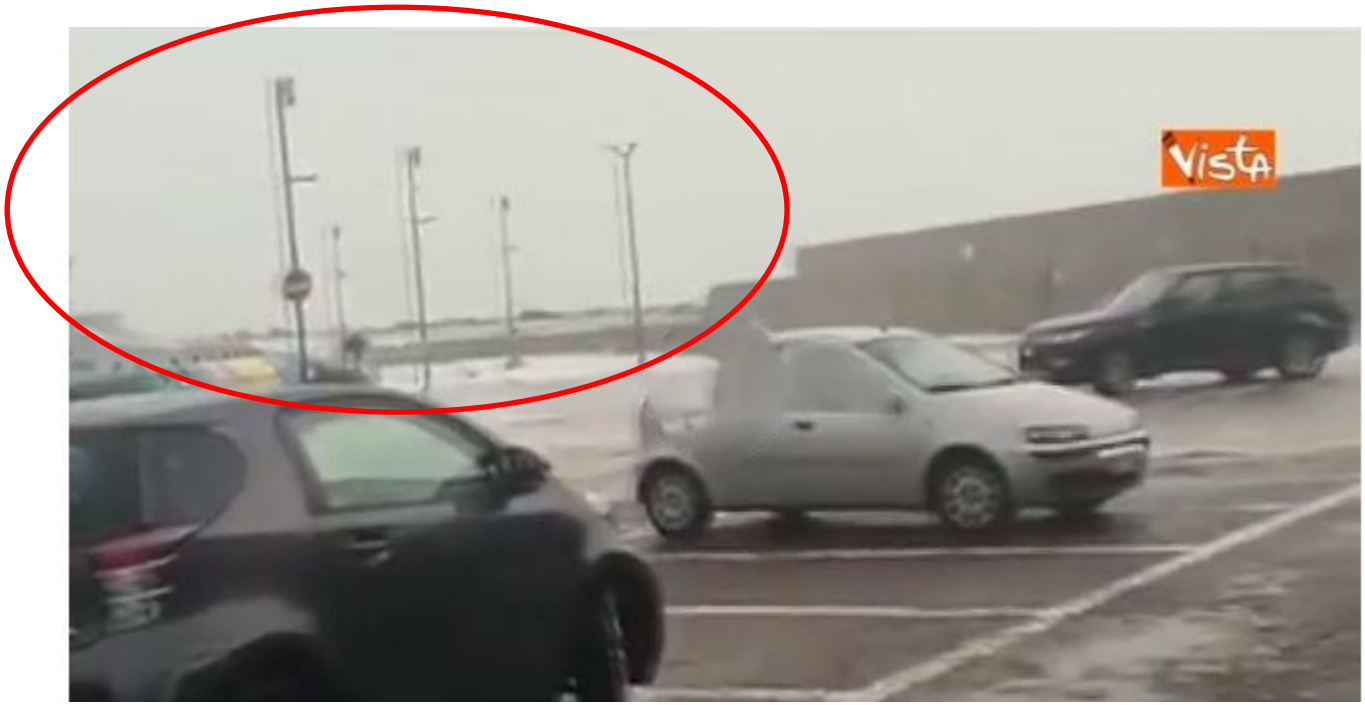

Effetti prodotti dalla mareggiata VAIA sul Tirreno meridionale

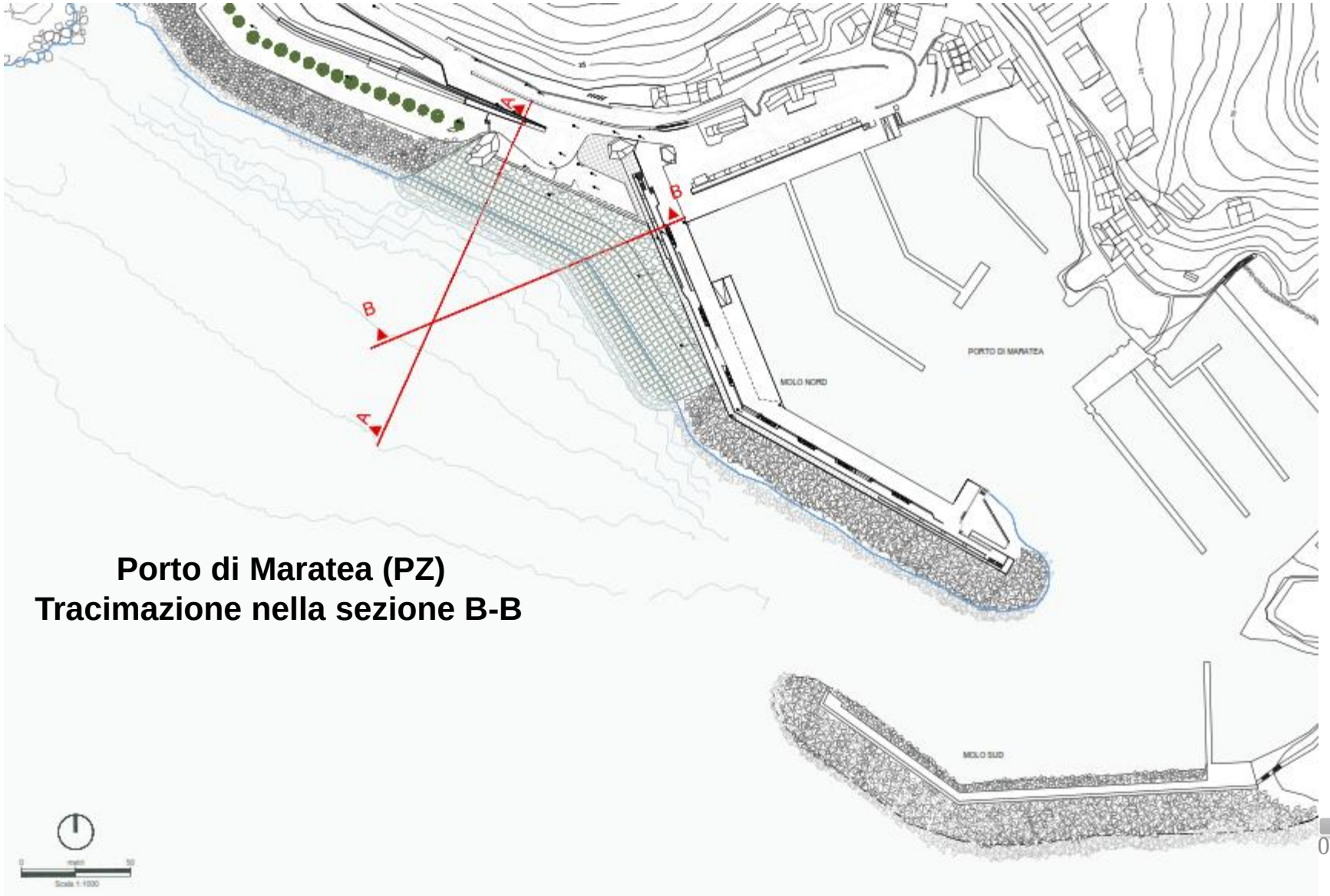

Porto di Maratea (PZ)
Tracimazione nella sezione B-B


Porto di Maratea (PZ)
Tracimazione della diga foranea

Effetti prodotti dalla mareggiata VAIA sul Tirreno meridionale

Torre del Greco – Litorale La Scala

Litorale La Scala – mareggiata ottobre 2018

Litorale La Scala – mareggiata ottobre 2018

Litorale La Scala – mareggiata ottobre 2018

MANTELLATA
1a Dislocamento unità
1b Slittamento
1c Rottura unità
1d Cedimento

FILTRO
2a Perdita materiale fino

BERMA AL PIEDE
3a Dislocamento unità

MANTELLATA RETROSTANTE
4a Dislocamento unità
4b Slittamento

CORONAMENTO
5a Slittamento
5b Rovesciamento
5c Frattura
5d Escavazione al piede

NUCLEO
6a Cedimento

SOTTOSUOLO
7a Cedimento - Deformazione
7b Erosione
7c Slittamento

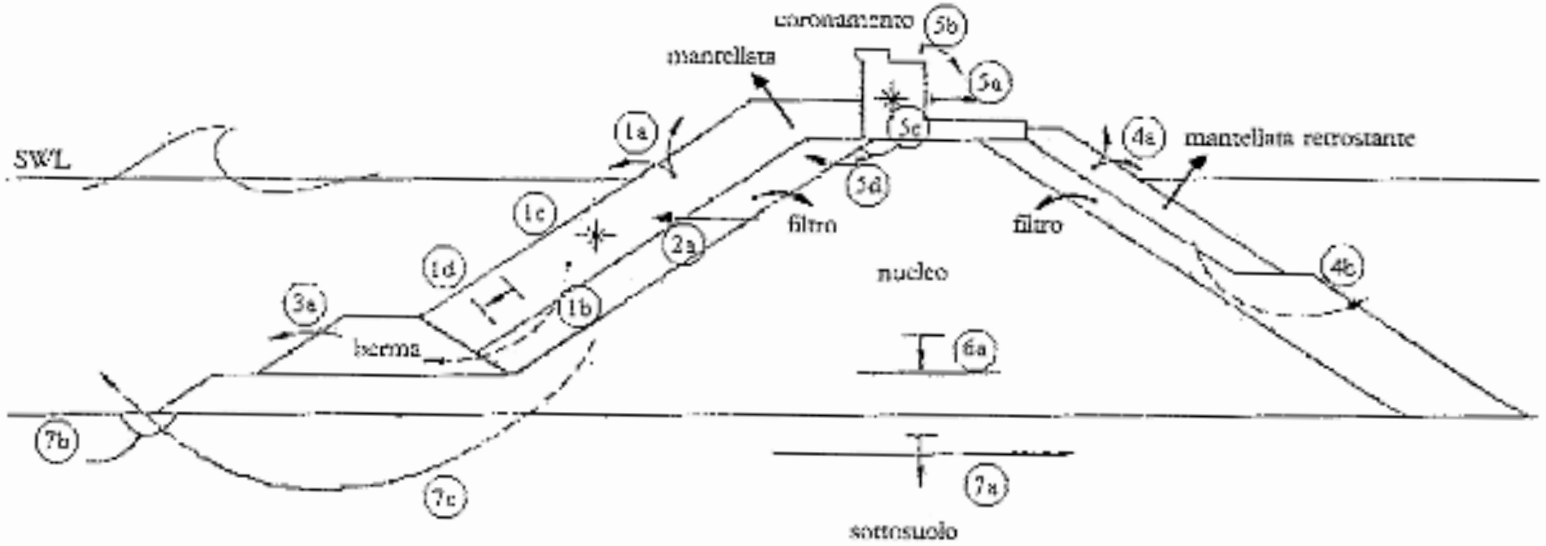

Figura 125 - Modalità di dissesto di una diga a scogliera (Burchart, 1992)

In Figura 125 sono schematizzati i possibili dissesti nelle varie parti dell'opera:

1. Dissesto dello strato di mantellata
   .1a Dislocamento degli elementi
   .1b Slittamento
   .1c Rottura degli elementi
   .1d Cedimento
2. Dissesto del filtro
   .2a Perdita del materiale più fine
3. Dissesto della berma al piede
   .3a Dislocamento degli elementi
4. Dissesto della mantellata retrostante (lato terra)
   .4a Dislocamento degli elementi
   .4b Slittamento
5. Dissesto del coronamento
   .5a Slittamento
   .5b Rovesciamento
   .5c Frattura
   .5d Escavazione al piede
6. Dissesto del nucleo
   .6a Cedimento
7. Dissesto al sottosuolo
   .7a Cedimento – Deformazione
   .7b Erosione
   .7c Slittamento

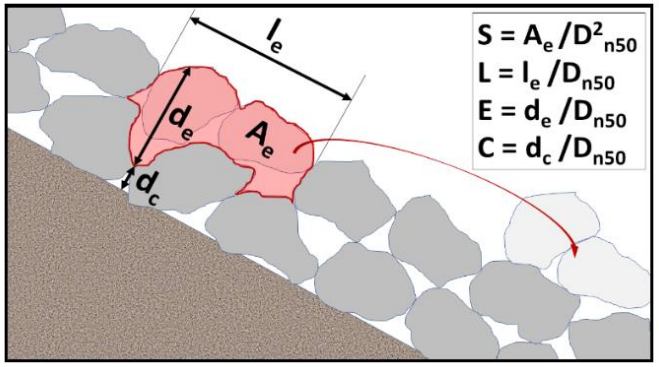

Campos et al, J. Mar. Sci. Eng. 2020, 8, 306; doi:10.3390/jmse8050306

2.2.1. S, Dimensionless Eroded Area

2.2.2. D%, Percentage Volume of Stones Eroded Relative to the Total Volume of stones in the Active Armor Layer

2.2.3. S_N, Dimensionless Eroded Area Accounting for Number of Displaced Units

The descriptor S can be re-formulated when visual methods are used;
The volume eroded from a section of width X can be expressed in terms of the average eroded area (Ve= Ae x X) or in terms of the number of displaced armor stones:

$$V_e = N_d D^3_{n50}/(1-n),$$

Where N_d is the number of displaced stones and n is the porosity.

$$S_N = \frac{N_d D_{n50}}{X(1-n)}$$

2.2.5. No, Number of Units Displaced out of the Armor Layer within a Strip Width of One Equivalent Cube Length

Van der Meer (1992) coined the term Nod for displacement and Nor for rocking

Table 1. Thresholds of S for different damage levels for non-overtopped two layers conventional breakwaters according to Vidal et al. [21] and the Rock Manual [2].

	DIMENSIONLESS EROSION AREA (S)						
	Threshold 1		Threshold 2–3			Threshold 4	
Cot α	Damage Initiation [21]	Start of Damage [2]	Iribarren's damage [21]	Initiation of destruction [21]	Intermediate Damage [2]	Destruction [21]	Failure [2]
1.5	1.5	2	2.5	6.5	3 to 5	12	8
2	2	2	3	8	4 to 6	14	8
3	2.5	2	3.5	9.5	6 to 9	16	12
4	3	3	4	11	8 to 12	18	17

Damage initiation and progression is a 3D process, even for breakwaters tested in a wave flume. The eroded units from a certain profile are not necessarily accreted at the bottom of the same profile, as they could roll down following a non-normal trajectory. In addition, the consequences of the extraction of units concentrated in a deep pocket are different from an extensive superficial removal. The spatial component and shape of damage is, therefore, crucial to understand this failure mode; nevertheless, the available descriptors up to date seem to be mainly focused on measuring an averaged magnitude on a 2D profile. Even damage descriptors derived from visual methods, which are based on a front view of the slope, are averaged over a longitudinal width or over an active region, loosing information such as the planar shape of the eroded area or the number of eroded pockets.

Musumeci et al., Measurement 117 (2018) 347–364

Musumeci et al. (2018) propose a novel three-dimensional laboratory technique based on RGB-D cameras to measure rubble-mound breakwater damage simultaneously above and below sea water level. In particular, here the proposed monitoring method is applied to the investigation of the stability of an Accropode breakwater under wave attack. The potentialities of the proposed technique are pointed out by using traditional and new methodologies to describe the structure damages.

In particular, Accropodes belong to the category of single-layer concrete armour blocks. They are quasi-randomly placed, according to a well-defined positioning of their centre of mass and to some construction rules-of-thumb aimed at ensuring the maximum level of interlocking [23]. Their behaviour is quite different from that of double layer elements. Indeed, the packing of the elements is completed under the wave attack and the system acts as an integral layer [5]. The work in Kobayashi and Kaihatsu [24] investigated experimentally the performance of Accropodes, reporting good stability characteristics for this type of blocks based also on field experience. However the authors underline the fact that although the stability at no damage condition was very high, the criteria of no damage and failure were very close. This was also confirmed by van der Meer [4], who suggests the following criteria for initiation of damage and failure respectively:

$$\frac{H_s}{\Delta D_n} = 3.7 \qquad \frac{H_s}{\Delta D_n} = 4.1$$

The stability of a traditional breakwater protected by an Accropode armour layer was investigated. The experiments were carried out at the Hydraulic Laboratory of the University of Catania. The wave tank is 18 m long, 3.60 m wide and 1.20 m deep. The flap-type wavemaker, located at one end of the flume, is electronically controlled and it is able to generate random waves with a given Jonswap spectrum. Tests were performed on two configurations of an Accropode breakwater, with different design of the toe of the structure, and in turn different stability properties of the armour layer. Both structures are attacked by series of sea states, made up by about 1500 irregular waves.

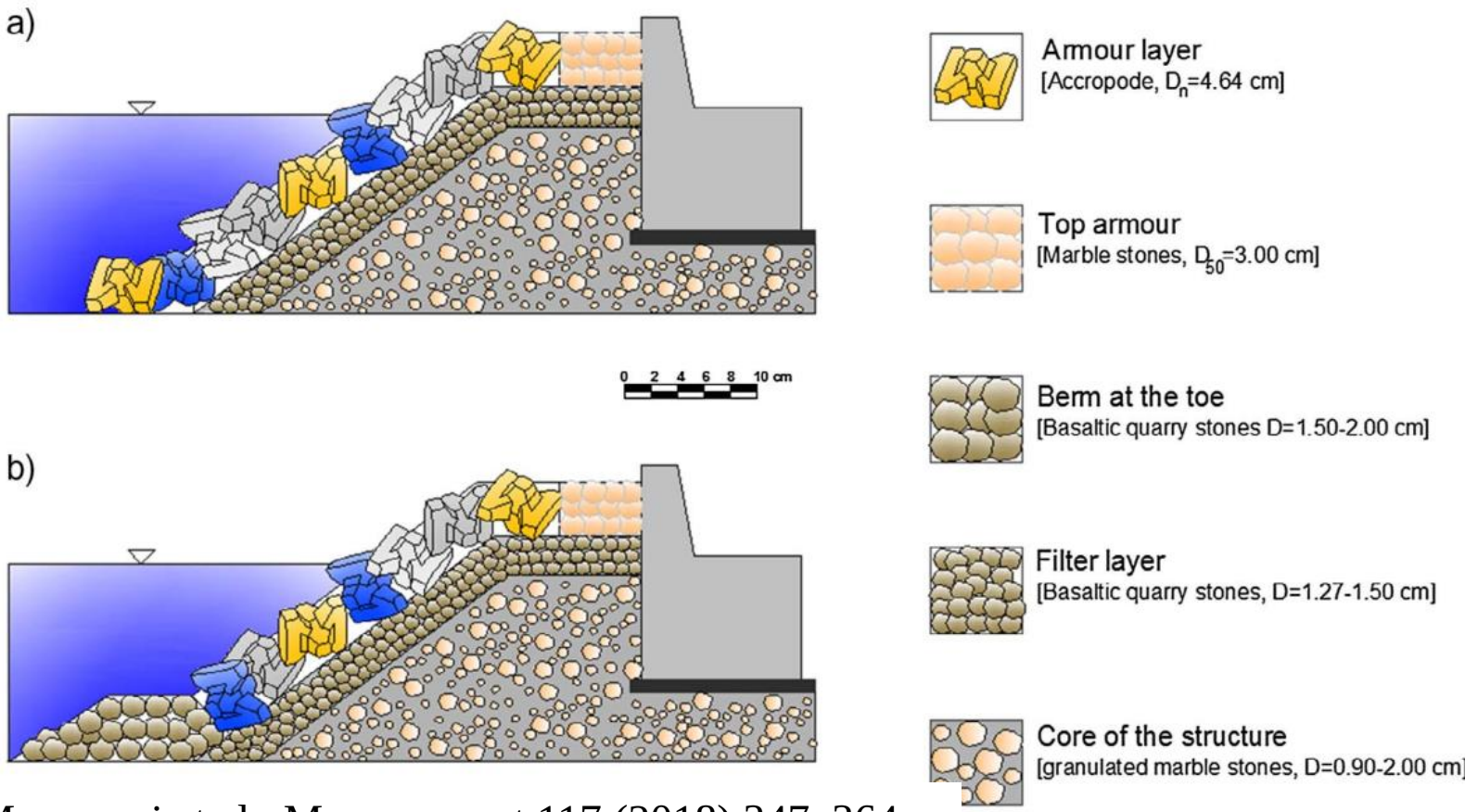

Musumeci et al., Measurement 117 (2018) 347–364

The widely known low-cost Microsoft Kinect camera was used as RGB-D camera in the experiments. Microsoft Kinect sensor belongs to the family of RGB-D devices which reconstruct the depth of a scene by using an infrared (IR) light pattern [36].
In order to create the depth map, the Kinect's IR projector throws a bundle of pseudo-random infrared beams. The reflected rays are captured by the infrared camera, and a 3D reconstruction algorithm determines how the points are close to the device. The depth map of the scene is provided as an image M of *m x n* size, where each pixel p(x.y) encodes the distance in the scene of the 3D point from the sensor.
The structured light technique used by the Kinect exploits a stereo vision system built by coupling the projector and the camera. A known infrared pattern is projected into the scene and the depth of the objects is computed by measuring its distortion on the objects.

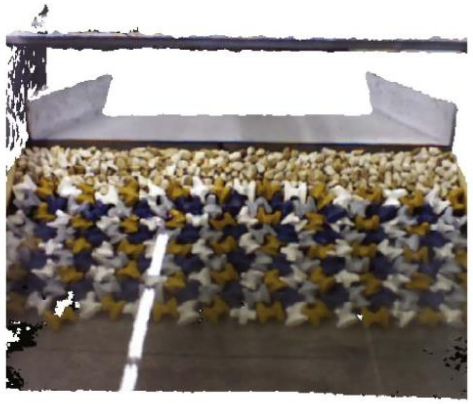

(a) A03

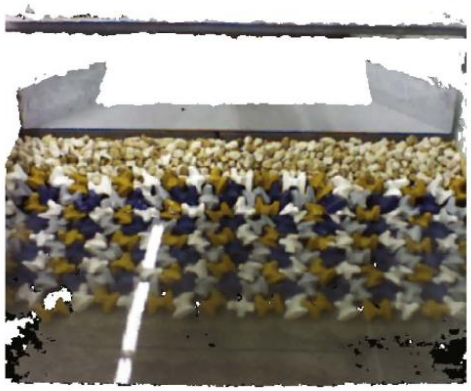

(b) A04

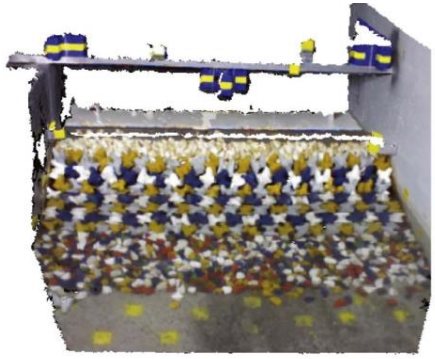

(a) B05

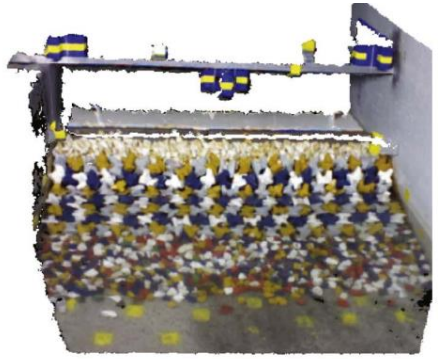

(b) B06

Musumeci et al., Measurement 117 (2018) 347–364

The damage endured by the structure, was visualised in terms of the Euclidean distance between the sampled control centroids (i. e. the control points obtained before the experiment started) and the centroids sampled at different instants during the test.

The N_{dc} value is a measure of the overall damage of the breakwater based on the centroids distance. More precisely, it indicates the percentage of centroids, for a given cloud, whose shift lies in one of the selected distance classes. Every class represents a distance interval. The intervals are obtained by equally dividing the maximum registered distance by the number n of classes.

The results on the rotational movements of the armour layer elements contribute to prove an incremental damage of the breakwater.

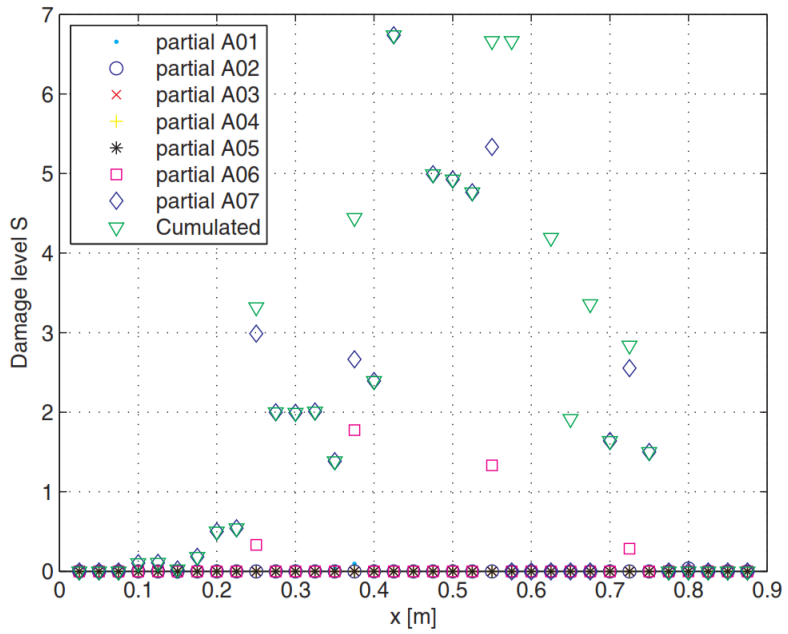

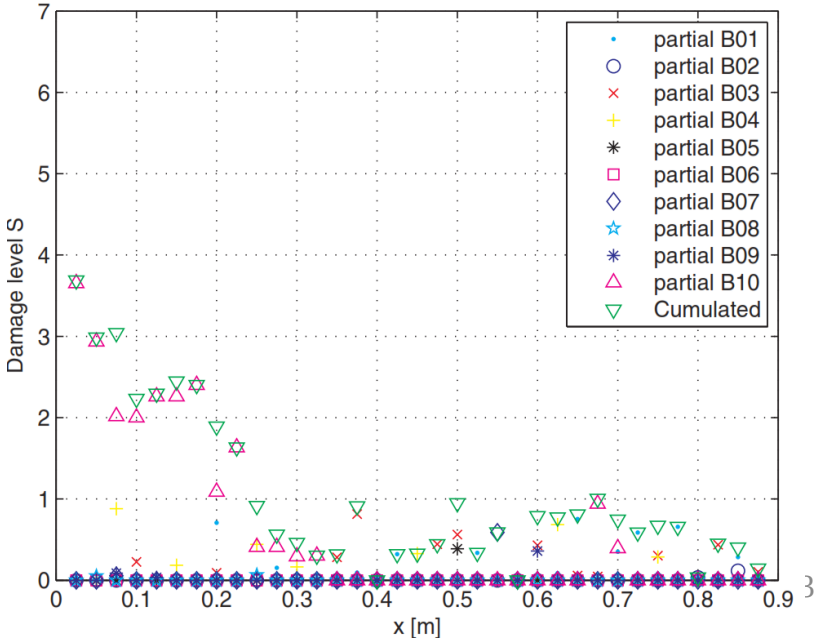

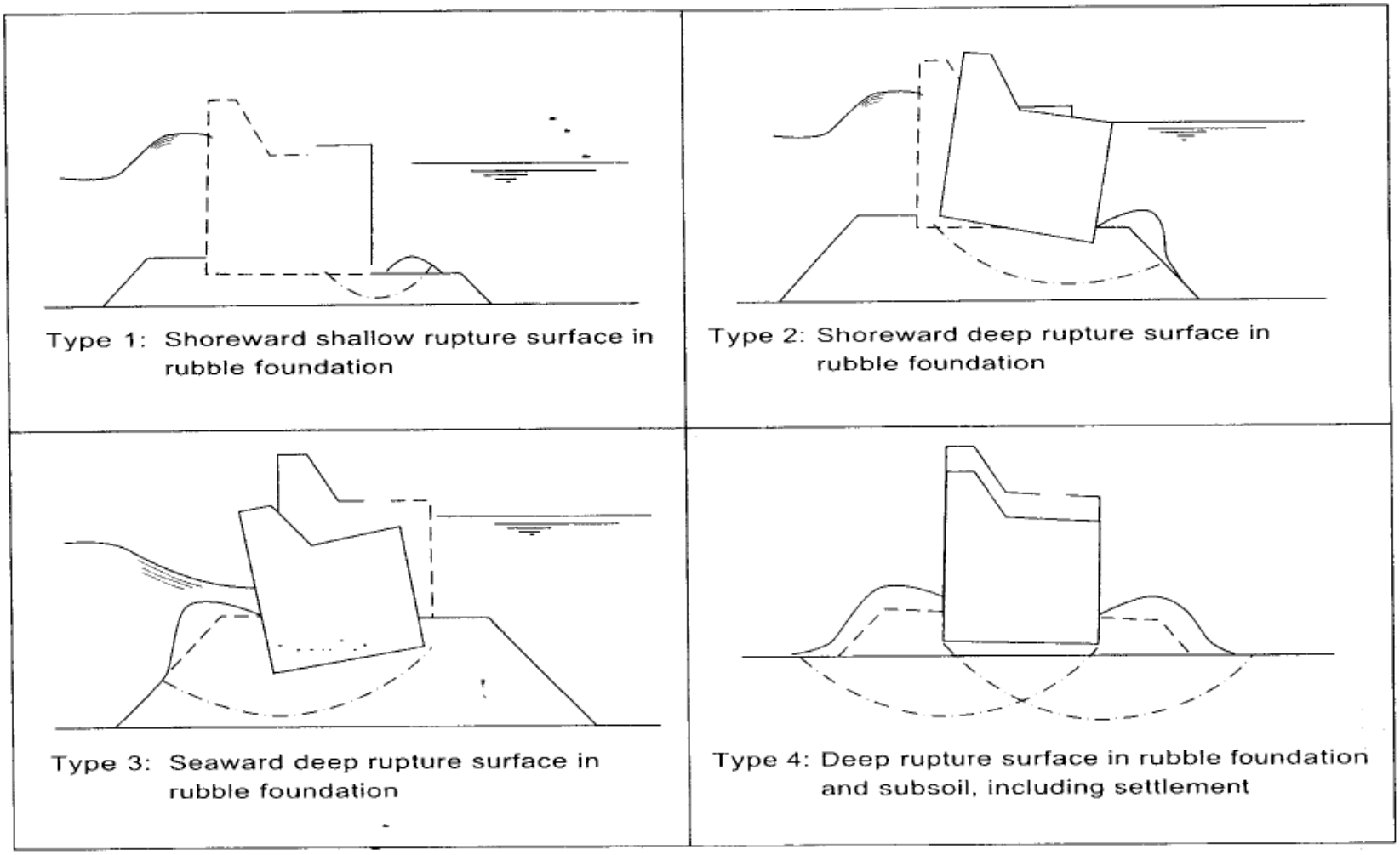

Fig. 7.45 Types of bearing capacity failure (adapted from Oumeraci et al., *2001)*

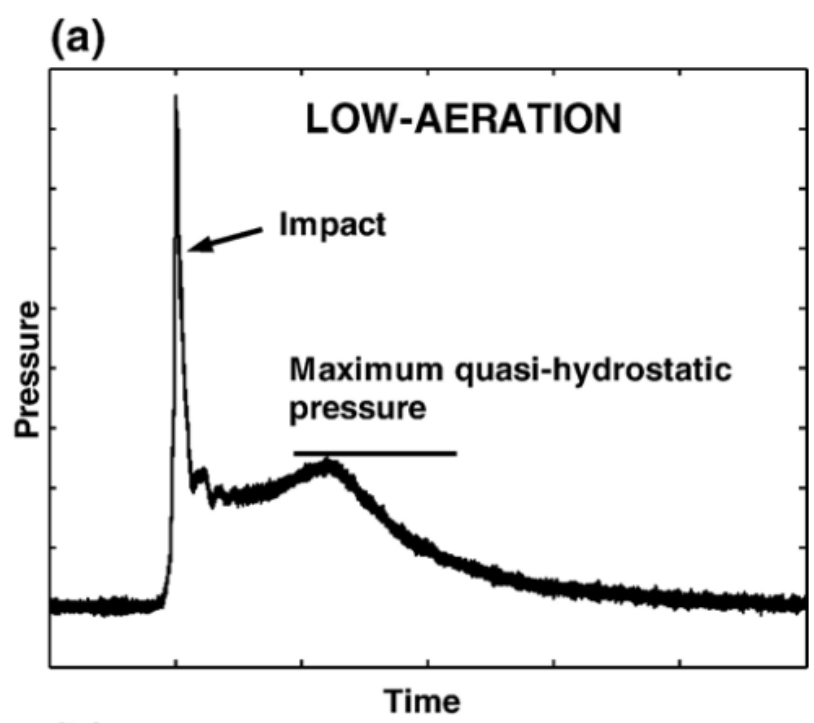
(a)
LOW-AERATION
Impact
Maximum quasi-hydrostatic pressure
Pressure
Time

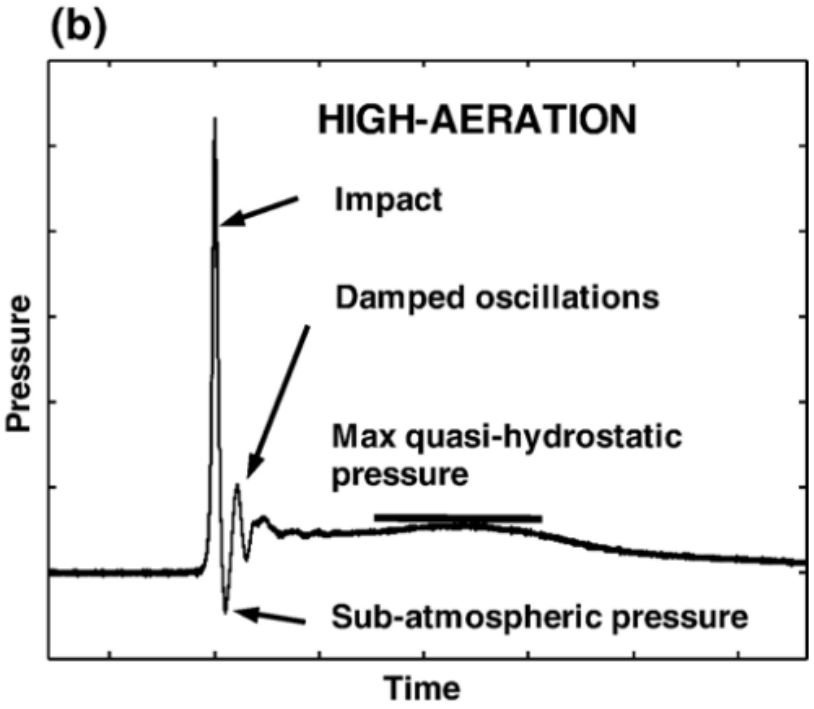
(b)
HIGH-AERATION
Impact
Damped oscillations
Max quasi-hydrostatic pressure
Sub-atmospheric pressure
Pressure
Time

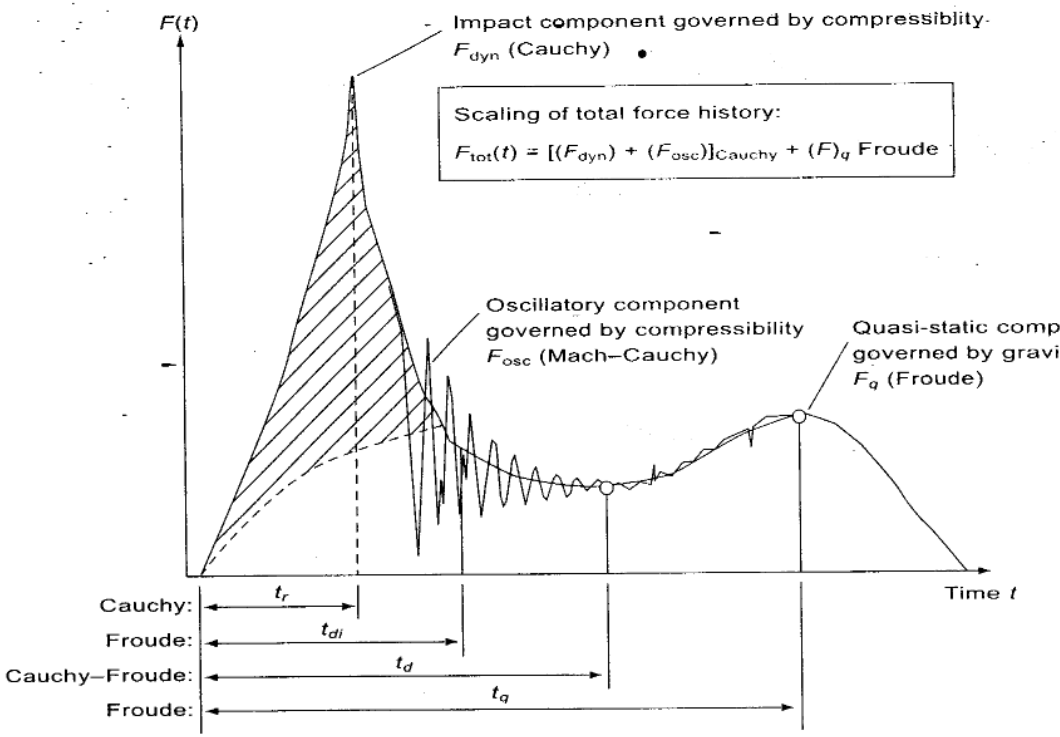
F(t)
Impact component governed by compressiblity
F_{dyn} (Cauchy)
Scaling of total force history:
$F_{tot}(t) = [(F_{dyn}) + (F_{osc})]_{Cauchy} + (F)_q$ Froude
Oscillatory component governed by compressibility
F_{osc} (Mach–Cauchy)
Quasi-static comp
governed by gravi
F_q (Froude)
Time t
Cauchy:
Froude:
Cauchy–Froude:
Froude:
t_r
t_{di}
t_d
t_q

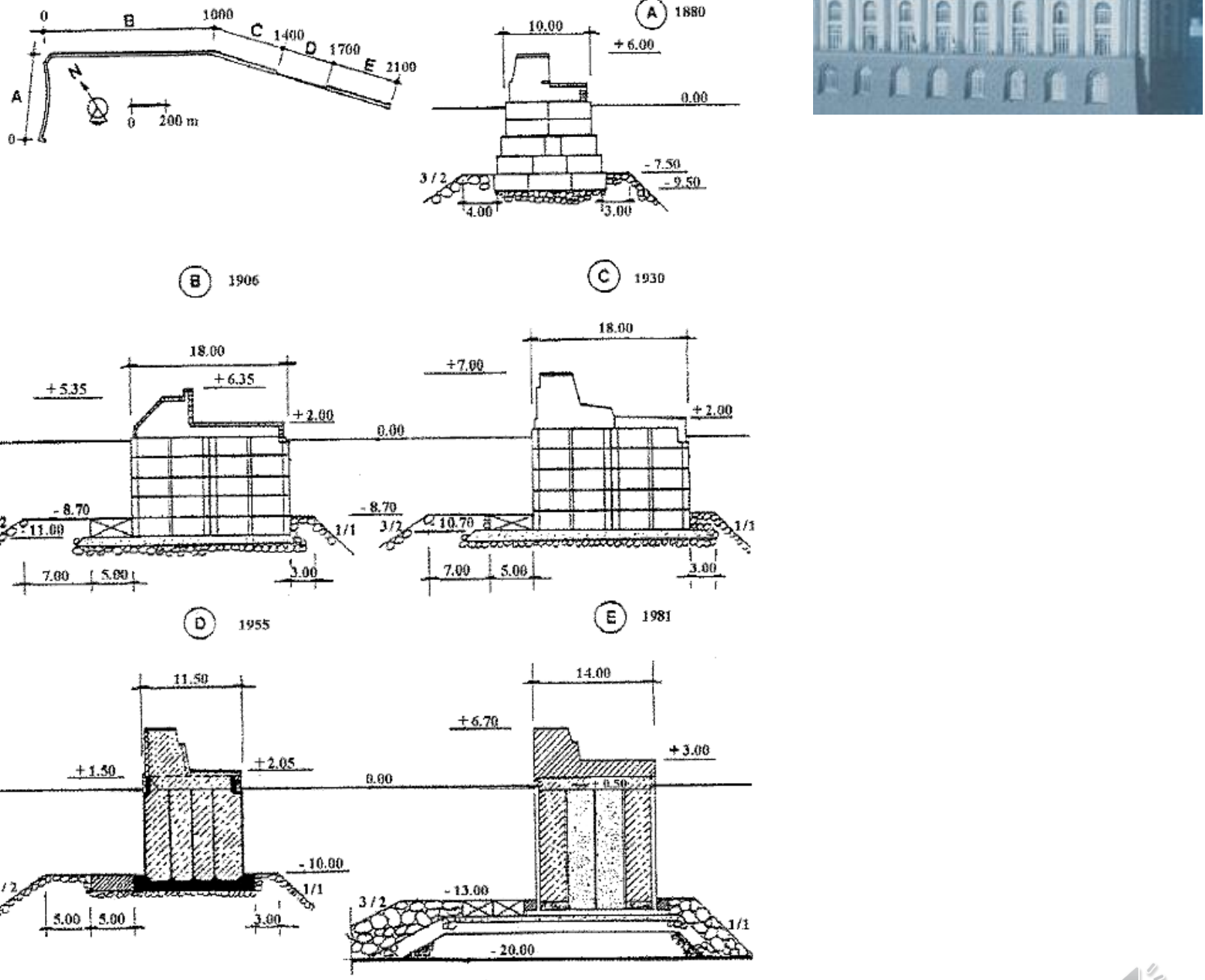

Figura 101 - Planimetria e sezioni della diga Duca d'Aosta di Napoli (da Franco e Passoni, 1992)

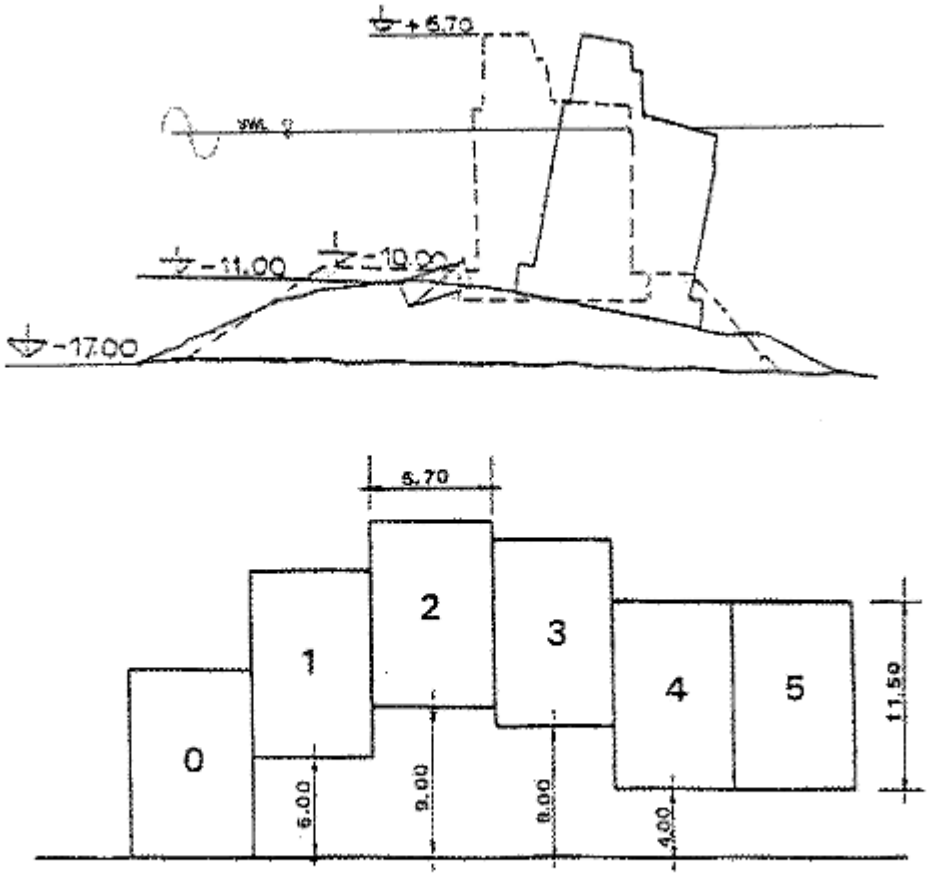

Figura 102 - Planimetria e sezione dei dissesti arrecati alla zona D della diga di Napoli (da Franco e Passoni, 1992)

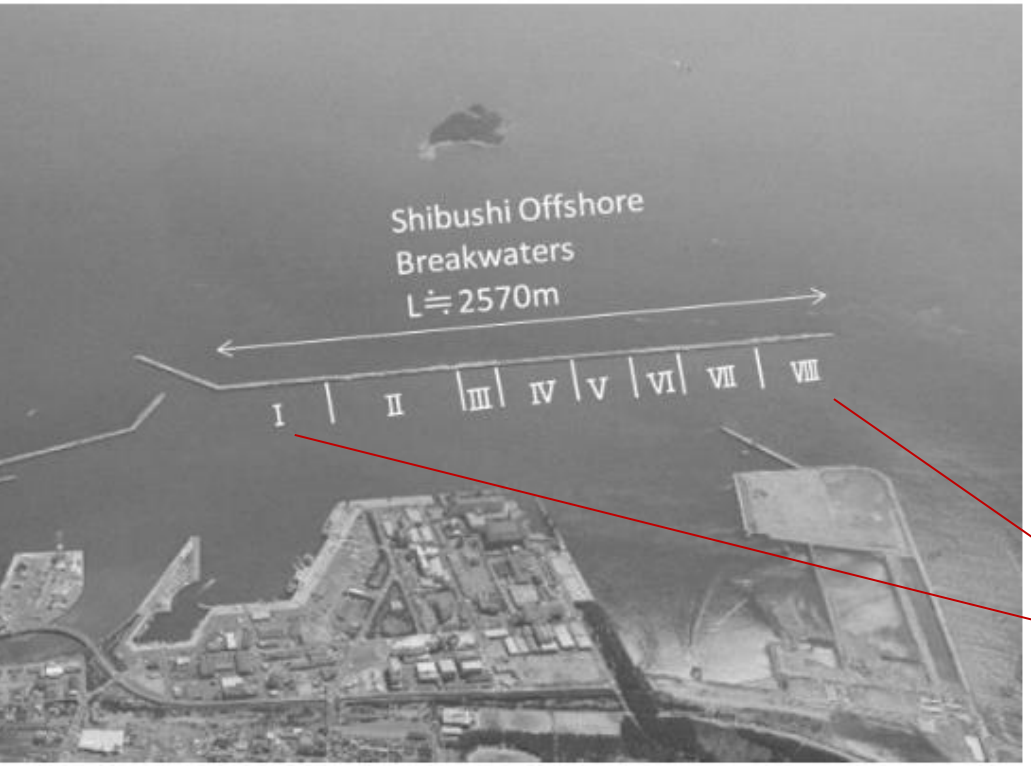

Fig. 1. Shibushi ports in the southern part of Japan.

Table 1. Cross-section of the Shibushi breakwaters.

Section	Caisson height (m)	Caisson width (incl. footing) (m)	Depth above original ground D.L. (m)	Depth above rubble mound D.L. (m)	Depth above foot protection D.L. (m)	Height of caisson above sea level D.L. (m)
II	15.5	18.5 (21.5)	−11.5	−8.5	−7.2	+7.0
III	15.5	19.1 (22.1)	−11.5	−8.5	−7.2	+7.0
IV	16.0	20.5 (23.5)	−12.4	−9.0	−7.7	+7.0
V	16.0	22.8 (25.8)	−13.2	−9.0	−7.7	+7.0
VI	16.0	24.9 (27.9)	−13.2	−9.0	−7.7	+7.0
VII	16.0	29.5 (35.5)	−15.0	−9.0	−7.7	+7.0

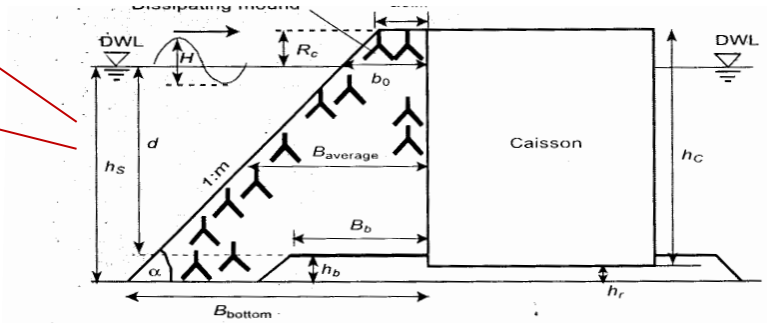

Fig. B9 Definition sketch for typical armoured caisson breakwater

Takagi et al. (2008) hanno verificato la stabilità del frangiflutti esistente di fronte al porto di Shibushi in Giappone che si trova nella parte meridionale dell' isola di Kyushu ed è regolarmente sottoposto ad onde molto grandi, in particolare durante la stagione dei tifoni. Il frangiflutti offshore che protegge il porto di Shibushi è lungo 2.570 m lungo il suo tratto rettilineo e ha 8 sezioni trasversali di diverse tipologie di cassoni, come mostrato in Fig. 1. Tra questi cassoni, quelli della sezione I e della sezione VIII sono dotati di una mantellata per la dissipazione delle onde davanti alla parete del cassone, mentre le altre sezioni (da II a VII) sono semplici frangiflutti a cassone verticale senza mantellata antistante [Takagi et al., 2008].

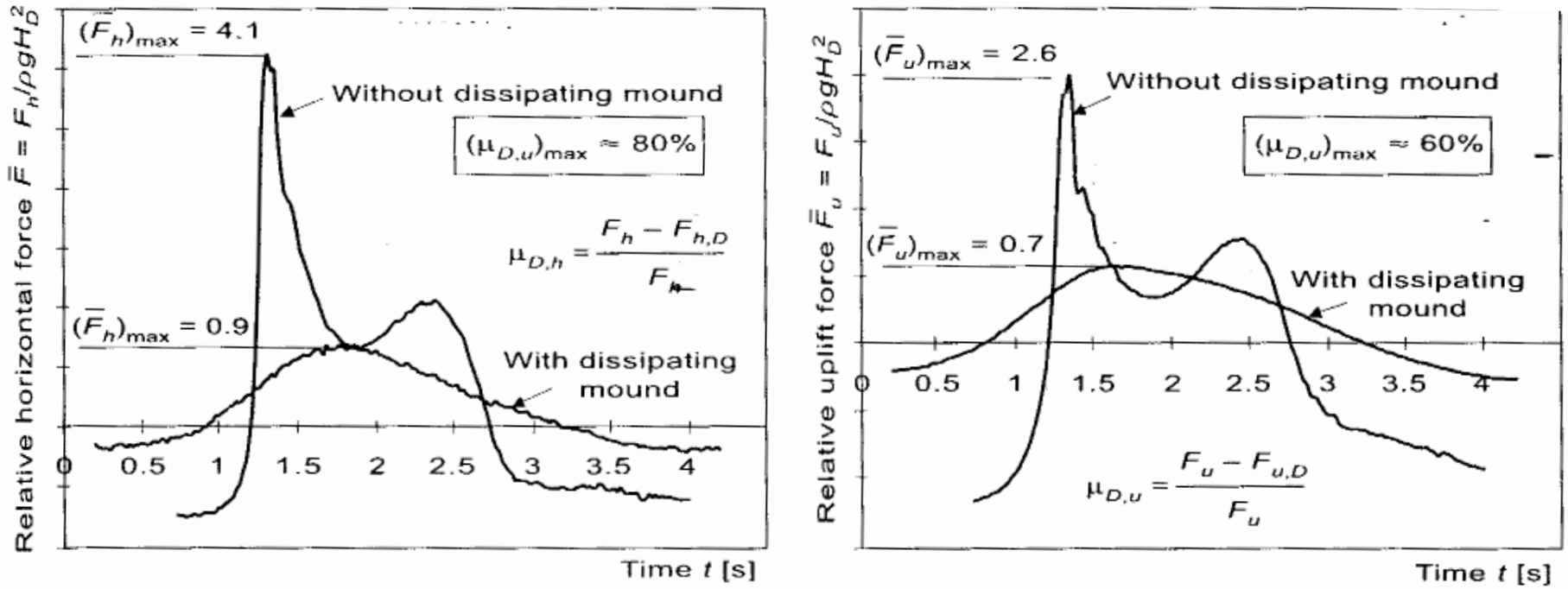

Fig. 7.40 Damping of pulsating wave impact loads by armouring (Kortenhaus and Oumeraci, 2000)

Takagi et al. (2008) hanno valutato la stabilità dei frangiflutti nelle condizioni di clima ondoso presenti e future al fine di stimare l'entità dell'accelerazione dei danni potenziali alle opere di protezione in base al futuro cambiamento climatico. L'aumento dell'altezza delle onde e del livello medio del mare porterebbe ad un aumento delle forze sul paramento verticale del frangiflutti, che si tradurrebbe in una maggiore distanza di dislocamento orizzontale e quindi una "accelerazione" del danno.
L'aumento del 10% della velocità del vento comporterebbe un aumento di Hs tra il 17 e il 25% rispetto alla stima dell'altezza significativa nel passato.

Table 5. Wave-height increase due to a 10% wind speed increase.

Typhoon No.	Observed $H_{1/3}$ (m)	Estimated $H_{1/3}$ (Komen) (m)	Estimated $H_{1/3}$ (Janssen) (m)	Applied model (regarding growth by wind)	Estimated (under climate change) (m)	Increase rate of wave height (%)
TY0206	4.4	5.5	4.1	Janssen	4.9	19.5
TY0207	3.7	6.2	4.0	Janssen	5.0	25.5
TY0209	5.1	5.9	4.1	Komen	6.9	16.9
TY0304	3.9	4.5	3.3	Janssen	4.1	24.2
TY0310	8.0	8.6	5.9	Komen	10.3	19.8
TY0406	7.1	7.9	5.8	Komen	9.4	19.0
TY0415	3.7	3.4	2.4	Komen	4.1	20.6
TY0416	9.0	12.3	9.2	Janssen	11.3	22.8
TY0418	6.3	7.0	4.8	Komen	8.4	20.0
TY0423	6.3	8.8	6.1	Janssen	7.5	23.0
					Mean	21.1

La distanza di scorrimento del cassone sullo scanno di imbasamento può essere calcolata dall'equazione del moto di un sistema rigido ad un grado di libertà. Takagi et al. [2007] hanno incorporato il termine della forza di smorzamento e hanno risolto l'equazione del moto.

$$(m + M_a)\ddot{x} = F_w(t) - F_f(t) - F_d(t)$$

in cui m è la massa del cassone, M_a è la massa aggiunta generata dall'acqua circostante il cassone, F_w è la forza di impatto dell' onda, F è la resistenza viscosa e F_d è la forza di smorzamento delle onde. M_a può essere espresso come

$$M_a = 1.0855\rho h^2 \, .$$

Risolvendo tale equazione, si può calcolare la distanza di scorrimento causata da ogni onda e successivamente si può ottenere la distanza totale di scorrimento sommando tutti questi contributi per tutta la durata di una tempesta. Sono state effettuate le simulazioni Montecarlo prendendo a base di calcolo dell' onda di riferimento offshore l'altezza d'onda di picco di 8,0 m e il corrispondente periodo d'onda di 13,7 sec (valori rilevati al picco della tempesta).

L'aumento medio futuro dell'altezza d'onda può essere considerato del 21,1% (vedi Tabella 5) e quindi l'altezza d'onda futura che risulterebbe da un aumento del 10% dell'intensità media del tifone di riferimento è stata calcolata di 9,7 m (= 8,0 × 1,211).

Il doppio impatto dell'innalzamento del livello del mare e dell'aumento dell'altezza d'onda dovuto ad una potenziale amplificazione in intensità di tifone sulla stabilità dei cassoni è stato valutato sulla base della "distanza di scorrimento attesa" calcolata con l'equazione precedente. Il concetto di distanza di scorrimento attesa dei frangiflutti a cassone è stata introdotta da Shimosako e Takahashi 2000] e successivamente è stato ampliato da altri ricercatori (Goda e Takagi [2000], Kim e Takayama [2003], Takagi et al. [2007, 2008], Esteban et al. [2007]).

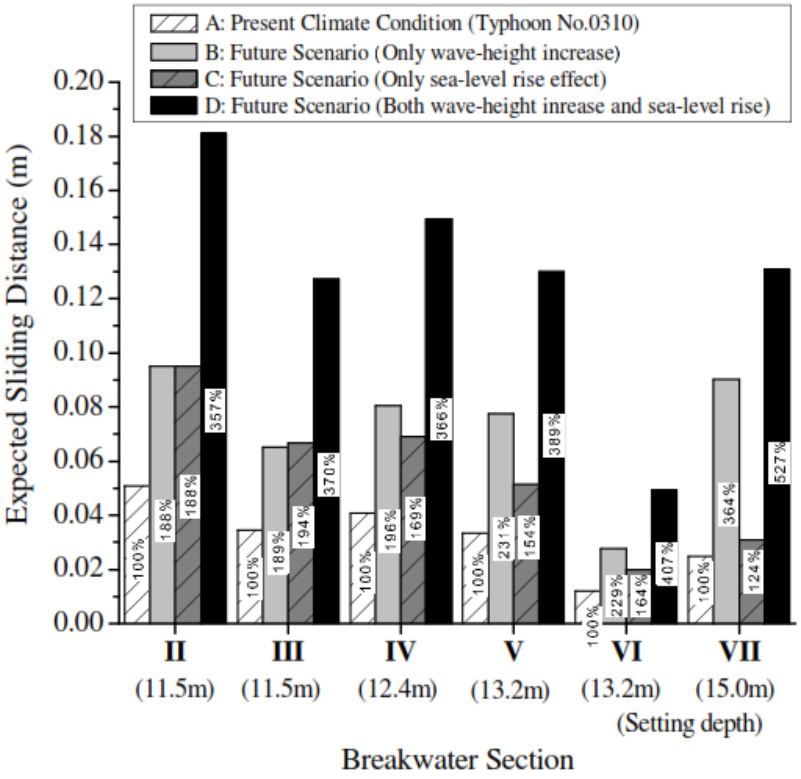

Effect of Climate Change on Performance-Based Design of Caisson Breakwaters

Kyung-Duck Suh, M.ASCE[1]; Seung-Woo Kim[2]; Nobuhito Mori, M.ASCE[3]; and Hajime Mase, M.ASCE[4]

JOURNAL OF WATERWAY, PORT, COASTAL, AND OCEAN ENGINEERING© ASCE / MAY/JUNE 2012

In this study, severe storm waves comparable with the design waves are assumed to occur approximately once a year (Goda and Takagi 2000; Shimosako and Takahashi 2000). The number of waves during a storm was assumed to be 1,000, which corresponds to approximately 3.2h for a design wave with Ts=14,0 s. The maximum accumulated sliding distance during the lifetime of the breakwater was set to Smax= þ+W/2, where b is the rear berm width of the riprap foundation, and W is the caisson width.

The performance-based design method was applied to the East Breakwater of the Port of Hitachinaka, located approximately 110 km northeast of central Tokyo. In this study, the breakwater was assumed to be completed in 2000, and the computations were made for t = 0–50 yrs, from 2000 to 2050. Unless otherwise stated, the sea-level rise from the A1B scenario was used, and a parabolic increase in wave height was assumed.

It was assumed that the importance of the breakwater is ordinary, so the allowable ESD is 0.3 m

Table 3. Allowable Exceedance Probability (%) of Allowable Sliding Distance (cm) by Japan Port and Harbour Association (2007) and Overseas Coastal Area Development Institute of Japan (2009)

Limit state (allowable sliding distance)	Importance of structure		
	High	Ordinary	Low
Repairable (10)	15	30	50
Ultimate (30)	5	10	20
Collapse (100)	2.5	5	10

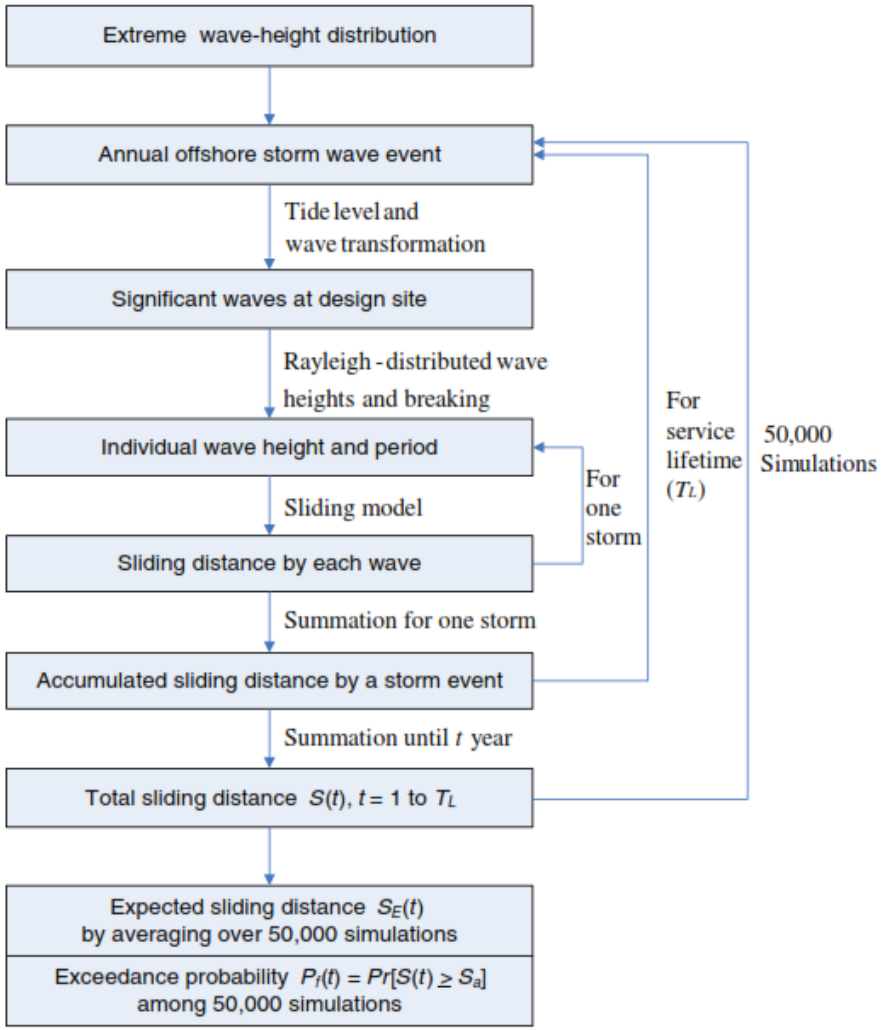

Tide and Storm Surge

With a tidal range of $\Delta\eta = 1.5$ m, the tide level η_t was simply assumed to vary sinusoidally between low water level (LWL) ($\eta_t = 0$) and high water level (HWL) ($\eta_t = \Delta\eta$). For simplicity, the effect of storm surge was taken into account by adding 10% of the deep-water significant wave height to the tide level (Shimosako and Takahashi 1998; Kim and Takayama 2003). This assumption corresponds to the wind set-up change owing to extreme wind stress change. Because the increase of wave height owing to climate change is taken into account, the influence of climate change on storm surge is also taken into account indirectly.

the top of the riprap foundation is 17.0 m. The crest elevation above LWL is 9.5 m. The slope of the front top of the caisson is 1:1. The seaward slope of the riprap foundation is covered with armor blocks of 122.5 kN, and the rear berm is 10.0-m wide.

Geometric Variables

The bottom slope near the Port of Hitachinaka varies from 1:80 to 1:100, with a depth of 10 m at 0.8 km offshore and a depth of 20 m at a distance 2.0 km offshore. The water depth at the breakwater site is 24.2 m (below LWL), and the breakwater is located approximately 2.6 km from the shoreline. The breakwater is 6-km long, is oriented in north-south direction, and is parallel to the shoreline. The predominant wave direction is normal to the breakwater. This study used cross section IV, as shown in Fig. 2, which is a typical sloping-top caisson breakwater. The bottom slope is 1:100, the caisson weight per unit length in air is 11,348 kN/m, and the buoyancy is 4,430 kN/m. The width of the caisson is 22.0 m. The distance from LWL to the bottom of the caisson is 18.5 m.

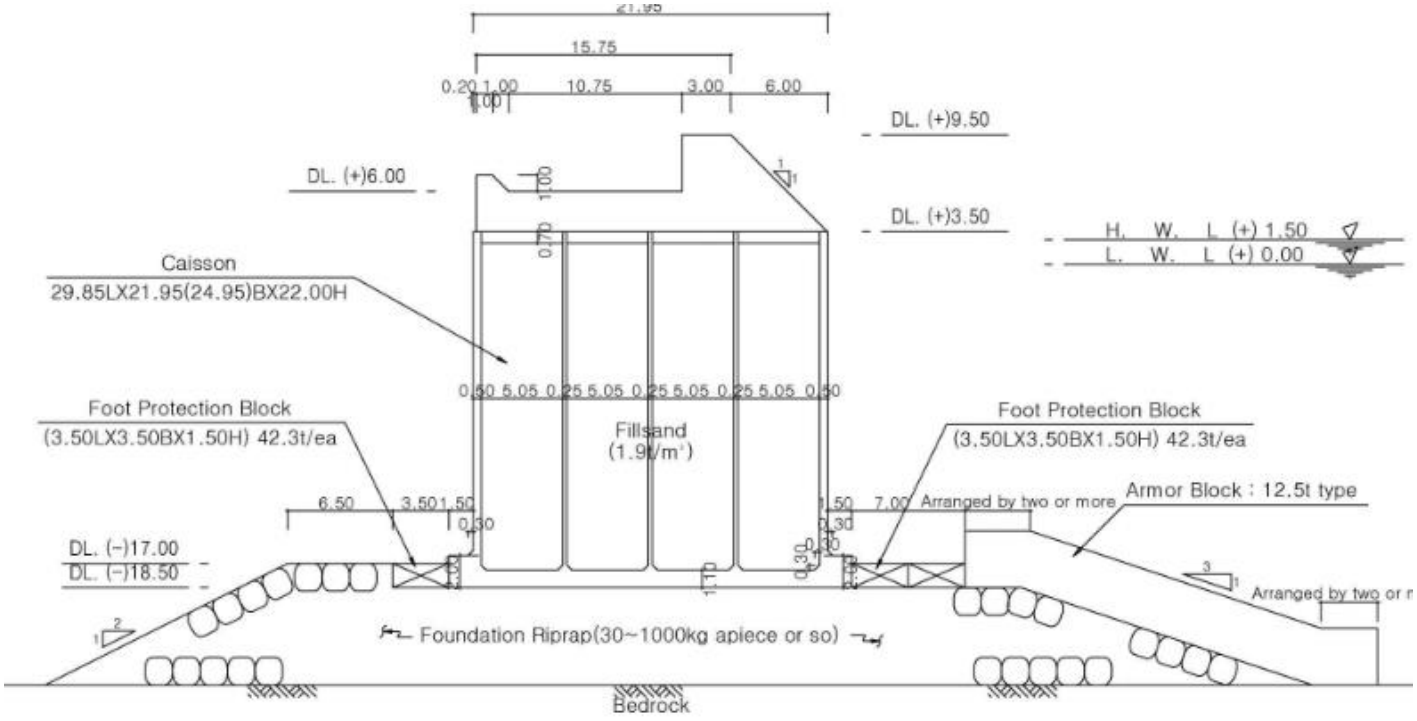

Fig. 2. Cross section IV of East Breakwater of Port of Hitachinaka

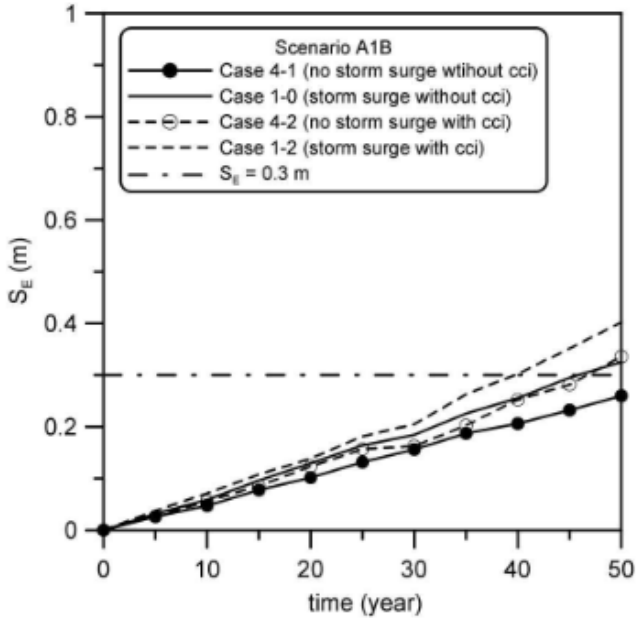

Fig. 7. Temporal variation of expected sliding distance for Case 4 (influence of storm surge)

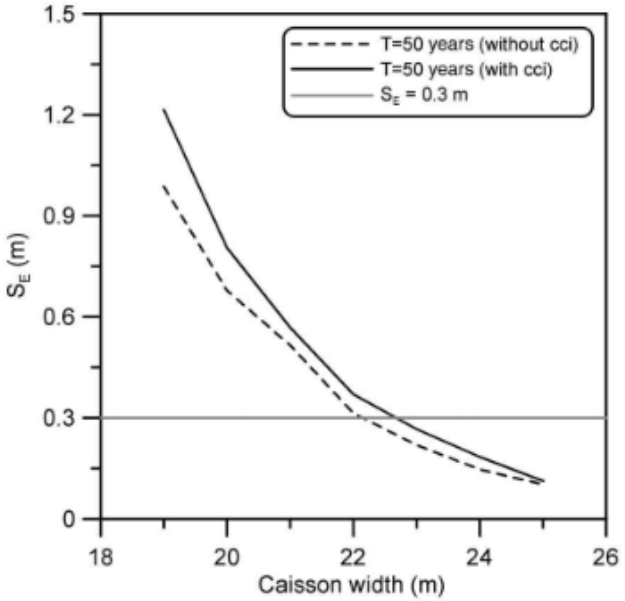

Fig. 10. Expected sliding distance versus caisson width for parabolic increase of wave height

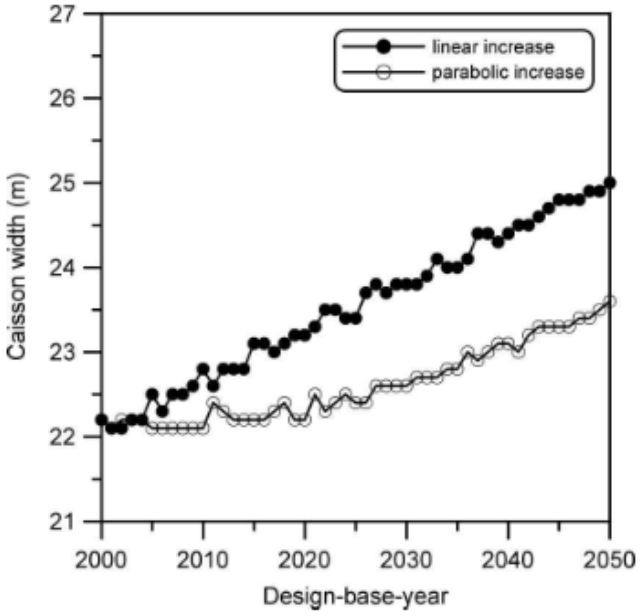

Fig. 14. Caisson width versus design-base-year calculated with expected sliding distance as the criterion

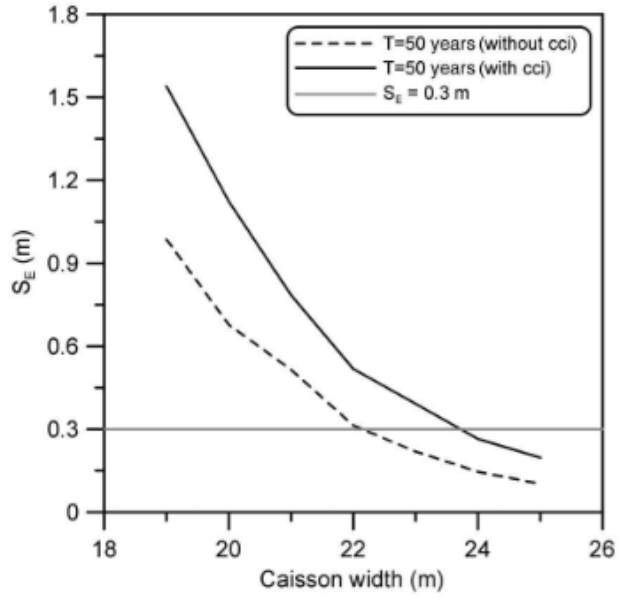

Fig. 12. Expected sliding distance versus caisson width for linear increase of wave height

CONCLUSIONS

Breakwaters play a crucial role in the protection of coastal zones.

Damage in **rubble mound breakwaters** is related to the hydraulic instability of the armor layer. Damage measurement technique proposed by Musumeci et al (2018) based on RGB-D cameras applied to the stability of an Accropode breakwater demonstrated a significant 3D behaviour of the element displacements.
Safety of the structure against extreme waves is achieved with a berm at the section base. This is crucial with Accropode units, which have a limited safety factor.

Damage in **vertical wall structures** consists essentially in the sliding of the caisson.
Assuming an allowable sliding distance of 30cm, the performance-based design method applied to a caisson breakwater showed that the increase in SWH and in SWL implies an increase of the caisson width to ensure breakwater stability. The same result is obtained through a rubble mound structure added on the caisson front.

Naples Shipping Week

MOS MARITIME ENGINEERING DIVISION UNIVERSITY of SALERNO

ATENA ASSOCIAZIONE ITALIANA DI TECNICA NAVALE

ORDINE DEGLI INGEGNERI DELLA PROVINCIA DI SALERNO

The INTERNATIONAL PROPELLER CLUB Port of Salerno

TEMPESTE ESTREME

Aspetti tecnici, gestionali ed assicurativi

27 Settembre 2022 ore 14.00
Stazione Marittima di Salerno

GRAZIE PER L'ATTENZIONE!